Research Article | Vol. 25, No. 9 | 1 May 2017 | OPTICS EXPRESS 9556
Optics EXPRESS

Thermal lensing effects on lateral leakage in GaN-based vertical-cavity surface-emitting laser cavities

EHSAN HASHEMI,[1] JÖRGEN BENGTSSON,[1] JOHAN GUSTAVSSON,[1] MARCO CALCIATI,[2] MICHELE GOANO,[2,3] AND ÅSA HAGLUND[1,*]

[1]*Photonics Laboratory, Department of Microtechnology and Nanoscience, Chalmers University of Technology, 41296 Gothenburg, Sweden*
[2]*IEIIT-CNR, Politecnico di Torino, 10129 Turin, Italy*
[3]*Department of Electronics and Telecommunications, Politecnico di Torino, 10129 Turin, Italy*
[*]*asa.haglund@chalmers.se*

Abstract: Lateral leakage of light has been identified as a detrimental loss source in many suggested and experimentally realized GaN-based VCSELs. In the present work we include thermal effects to realistically account for the substantial Joule heating in these devices. In contrast to what could be expected from the previous results, the induced thermal lensing does not make antiguided cavities more positively guided, so that they approach the unguided regime with extremely high lateral leakage. Rather, thermal lensing strongly suppresses lateral leakage for both antiguided and guided cavities. This is explained in terms of lowered launch of power from the central part of the cavity and/or lower total internal reflection in the peripheral part; the former effect is active in all cavities whereas the latter only contributes to the very strongly reduced leakage in weakly antiguided cavities. Thermal lensing suppresses lateral leakage both for the fundamental and the first higher order mode, but a strong modal discrimination is still achieved for the antiguided cavities. Thus, strongly antiguided cavities could be used to achieve single-mode devices, but at the cost of slightly higher threshold gain and stronger temperature dependent performance characteristics.

OCIS codes: (140.5960) Semiconductor lasers; (140.7260) Vertical cavity surface emitting lasers; (140.7300) Visible lasers; (350.6830) Thermal lensing.

References and links

1. G. Cosendey, A. Castiglia, G. Rossbach, J. F. Carlin, and N. Grandjean, "Blue monolithic AlInN-based vertical cavity surface emitting laser diode on free-standing GaN substrate," Appl. Phys. Lett. **101**(15), 151113 (2012).
2. T. C. Lu, S. W. Chen, T. T. Wu, P. M. Tu, C. K. Chen, C. H. Chen, Z. Y. Li, H. C. Kuo, and S. C. Wang, "Continuous wave operation of current injected GaN vertical cavity surface emitting lasers at room temperature," Appl. Phys. Lett. **97**(7), 071114 (2010).
3. D. Kasahara, D. Morita, T. Kosugi, K. Nakagawa, J. Kawamata, Y. Higuchi, H. Matsumura, and T. Mukai, "Demonstration of blue and green GaN-based vertical-cavity surface-emitting lasers by current injection at room temperature," Appl. Phys. Express **4**(7), 072103 (2011).
4. T. Onishi, O. Imafuji, K. Nagamatsu, M. Kawaguchi, K. Yamanaka, and S. Takigawa, "Continuous wave operation of GaN vertical cavity surface emitting lasers at room temperature," IEEE J. Quantum Electron. **48**(9), 1107–1112 (2012).
5. W. J. Liu, X. L. Hu, L. Y. Ying, J. Y. Zhang, and B. P. Zhang, "Room temperature continuous wave lasing of electrically injected GaN-based vertical cavity surface emitting lasers," Appl. Phys. Lett. **104**(25), 251116 (2014).
6. G. Weng, Y. Mei, J. P. Liu, W. Hofmann, L. Y. Ying, J. Y. Zhang, Y. K. Bu, Z. C. Li, H. Yang, and B. P. Zhang, "Low threshold continuous-wave lasing of yellow-green InGaN-QD vertical-cavity surface-emitting lasers," Opt. Express **24**(14), 15546–15553 (2016).
7. J. T. Leonard, D. A. Cohen, B. P. Yonkee, R. M. Farrell, T. Margalith, S. Lee, S. P. DenBaars, J. S. Speck, and S. Nakamura, "Nonpolar III-nitride vertical-cavity surface-emitting lasers incorporating an ion implanted aperture," Appl. Phys. Lett. **107**(1), 011102 (2015).
8. J. T. Leonard, E. C. Young, B. P. Yonkee, D. A. Cohen, T. Margalith, S. P. DenBaars, J. S. Speck, and S. Nakamura, "Demonstration of a III-nitride vertical-cavity surface-emitting laser with a III-nitride tunnel junction intracavity contact," Appl. Phys. Lett. **107**(9), 091105 (2015).

#284573 https://doi.org/10.1364/OE.25.009556
Journal © 2017 Received 12 Jan 2017; revised 6 Apr 2017; accepted 11 Apr 2017; published 18 Apr 2017

Optics EXPRESS

9. J. T. Leonard, B. P. Yonkee, D. A. Cohen, L. Megalini, S. Lee, J. S. Speck, S. P. DenBaars, and S. Nakamura, "Nonpolar III-nitride vertical-cavity surface-emitting laser with a photoelectrochemically etched air-gap aperture," Appl. Phys. Lett. **108**(3), 031111 (2016).
10. T. Hamaguchi, N. Fuutagawa, S. Izumi, M. Murayama, and H. Narui, "Milliwatt-class GaN-based blue vertical-cavity surface-emitting lasers fabricated by epitaxial lateral overgrowth," Phys. Stat. Sol. A **213**(5), 1170–1176 (2016).
11. K. Ikeyama, Y. Kozuka, K. Matsui, S. Yoshida, T. Akagi, Y. Akatsuka, N. Koide, T. Takeuchi, S. Kamiyama, M. Iwaya, and I. Akasaki, "Room-temperature continuous-wave operation of GaN-based vertical-cavity surface-emitting lasers with n-type conducting AlInN/GaN distributed Bragg reflectors," Appl. Phys. Express **9**(10), 102101 (2016).
12. E. Hashemi, J. Bengtsson, J. Gustavsson, M. Stattin, G. Cosendey, N. Grandjean, and Å. Haglund, "Analysis of structurally sensitive loss in GaN-based VCSEL cavities and its effect on modal discrimination," Opt. Express **22**(1), 411-426 (2014).
13. J. Piprek, Z. M. Li, R. Farrell, S. P. DenBaars, and S. Nakamura, "Electronic Properties of InGaN/GaN Vertical-Cavity Lasers," in *Nitride Semiconductor Devices: Simulations and Principles,* J. Piprek, ed. (Wiley, 2007).
14. J. Piprek, "What is the problem with GaN-based VCSELs?" *Proc. International Conference on Numerical Simulation of Optoelectronic Devices* (IEEE, 2013), pp. 89–90.
15. D. M. Kuchta, A. V. Rylyakov, C. L. Schow, J. E. Proesel, C. W. Baks, P. Westbergh, J. S. Gustavsson, and A. Larsson, "A 50 Gb/s NRZ Modulated 850 nm VCSEL Transmitter Operating Error Free to 90°C," J. Lightwave Technol. **33**(4), 802–810 (2015).
16. K. Matsui, T. Furuta, N. Hayashi, Y. Kozuka, T. Akagi, T. Takeuchi, S. Kamiyama, M. Iwaya, and I. Akasaki, "3-mW RT-CW GaN-Based VCSELs and Their Temperature Dependence," presented at the International Workshop on Nitride Semiconductors, Orlando, USA, 2–7 Oct. 2016.
17. E. Hashemi, J. Gustavsson, J. Bengtsson, M. Stattin, G. Cosendey, N. Grandjean, and Å. Haglund, "Engineering the lateral optical guiding in gallium nitride-based vertical-cavity surface-emitting laser cavities to reach the lowest threshold gain," Jap. J. Appl. Phys. **52**(8S), 08JG04 (2013).
18. G. R. Hadley, "Effective index model for vertical-cavity surface-emitting lasers," Opt. Lett. **20**(13), 1483–1485 (1995).
19. T. Czyszanowski, M. Wasiak, R. P. Sarzała, and W. Nakwaski, "Exactness of simplified scalar optical approaches in modeling a threshold operation of possible nitride vertical-cavity surface-emitting lasers," Phys. Stat. Sol. A **204**(10), 3562–3573 (2007).
20. R. Sarzała, T. Czyszanowski, M. Wasiak, M. Dems, L. Piskorski, W. Nakwaski, and K. Panajotov, "Numerical self-consistent analysis of VCSELs," Adv. Opt. Technol. **2012**, 689519 (2012).
21. E. Hashemi, J. Bengtsson, J. Gustavsson, M. Stattin, M. Glauser, G. Cosendey, N. Grandjean, M. Calciati, M. Goano, and Å. Haglund, "Triggering of guiding and antiguiding effects in GaN-based VCSELs," Proc. SPIE **9001**, 90010A (2014).
22. M. Ohya, K. Fukuda, I. Masumoto, S. Kohmoto, K. Naniwae, M. Yamada, M. Matsudate, T. Tsukuda, T. Akagawa, and C. Sasaoka, "High-power operation of inner-stripe GaN-based blue-violet laser diodes," Proc. SPIE **6485**, 648505 (2007).
23. W. S. Tan, K. Takahashi, V. Bousquet, A. Ariyoshi, Y. Tsuda, M. Ohta, and M. Kauer, "Blue-violet inner stripe laser diodes using lattice matched AlInN as current confinement layer for high power operation," Appl. Phys. Express **2**(11), 112101 (2009).
24. B. S. Cheng, Y. L. Wu, T. C. Lu, C. H. Chiu, C. H. Chen, P. M. Tu, H. C. Kuo, S. C. Wang, and C. Y. Chang, "High Q microcavity light emitting diodes with buried AlN current apertures," Appl. Phys. Lett. **99**(4), 041101 (2011).
25. Y. Y. Lai, S. C. Huang, T. L. Ho, T. C. Lu, and S. C. Wang, "Numerical analysis on current and optical confinement of III-nitride vertical-cavity surface-emitting lasers," Opt. Express **22**(8), 9789–9797 (2014).
26. P. Śpiewak, A. K. Sokół, M. Wasiak, and R. P. Sarzała, "Impact of AlN-aperture on optical and electrical properties on nitride VCSEL," *Proc. International Conference on Numerical Simulation of Optoelectronic Devices* (IEEE, 2016), pp. 41–42.
27. J. F. Carlin, C. Zellweger, J. Dorsaz, S. Nicolay, G. Christmann, E. Feltin, R. Butté, and N. Grandjean, "Progresses in III-nitride distributed Bragg reflectors and microcavities using AlInN/GaN materials," Phys. Stat. Sol. B **242**(11), 2326–2344 (2005).
28. D. Brunner, H. Angerer, E. Bustarret, F. Freudenberg, R. Höpler, R. Dimitrov, O. Ambacher, and M. Stutzmann, "Optical constants of epitaxial AlGaN films and their temperature dependence," J. Appl. Phys., **82**(10), 5090–5096 (1997).
29. W. Nakwaski, T. Czyszanowski, and R. P. Sarzała, "Optical design of Vertical-Cavity Lasers," in *Nitride Semiconductor Devices: Simulations and Principles,* J. Piprek, ed. (Wiley, 2007).
30. N. Watanabe, T. Kimoto, and J. Suda, "Thermo-optic coefficients of SiC, GaN, and AlN up to 512°C from infrared to ultraviolet region for tunable filter applications," Proc. SPIE **7926**, 792604, (2011).
31. R. Hui, Y. Wan, J. Li, S. Jin, J. Lin, and H. Jiang, "III-nitride-based planar lightwave circuits for long wavelength optical communications," IEEE J. Quantum Electron. **41**(1), 100–110 (2005).
32. L. Redaelli, H. Wenzel, M. Martens, S. Einfeldt, M. Kneissl, and G. Tränkle, "Index antiguiding in narrow ridge-waveguide (In,Al)GaN-based laser diodes," J. Appl. Phys. **114**(11), 113102 (2013).

Optics EXPRESS

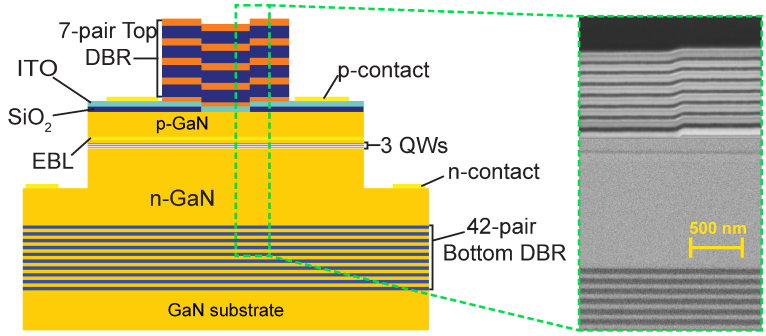

Fig. 1. Left: Schematic cross-sectional view of a VCSEL with a step in the layer profile. Right: Scanning electron microscopy (SEM) image of the layer structure in a fabricated GaN/AlInN-based VCSEL [1].

1. Introduction

Efficient current injection and lateral current confinement remain as major challenges in nitride-based vertical-cavity surface-emitting lasers (VCSELs) for blue-green emission [1–11]. Suggested and experimentally realized cavity structures often employ dielectric apertures to confine the current to the central region. More recently, buried tunnel junctions (BTJ) have been suggested, serving a similar purpose while also potentially improving the current spreading and simplify contacting to metals, since n-doped nitride material can be used in the upper part of the cavity instead of highly resistive p-doped material. Naturally, these effects have been more focused on the electrical rather than the optical properties. To achieve electrically injected VCSELs, it is however also important to consider how electrical apertures affect the optical properties of the VCSEL to achieve devices with low threshold gain and thus low threshold currents. We previously showed that, at least for a cold cavity, extremely small changes in the cavity design can lead to a dramatic change in the threshold gain [12]. More precisely, we studied the effects of the step in the layer structure of the cavity that naturally occurs when realizing a circular current aperture or BTJ. In both cases, the cavity structure is changed near the top mirror, because of the longitudinal displacement of the central part, near the optical axis, relative to the peripheral part. This occurs because the realization of the aperture/BTJ in general includes the formation of a stepped surface profile at the position of the aperture/BTJ onto which the layers of the top distributed Bragg reflector (DBR) mirror are then deposited. Unless special measures are taken in the processing, the stepped profile is very nearly preserved throughout the top mirror [1], see Fig. 1, and will therefore influence the optical behavior. In our previous study we showed that nanometer-sized changes in the step height in the profile can change a cavity from guided to antiguided, leading to massive lateral leakage, i.e. resonantly enhanced optical loss caused by light escaping in the radial direction. The conclusion was then that any suggested cavity structure should be checked, if not with the more rigorous 3D methods we used, at least with the computationally much less demanding effective refractive index method. The latter method gives as result the effective refractive index difference Δn_{eff} between the central and peripheral part of the cavity. We showed that the condition $\Delta n_{\mathrm{eff}}=0$, i.e. the boundary between antiguided ($\Delta n_{\mathrm{eff}} < 0$) and guided ($\Delta n_{\mathrm{eff}} > 0$) cavity in the effective refractive index sense, very accurately corresponds to the onset of excessive lateral leakage, which remains high for all antiguided cavities. To provide some safety margin, we argued that a value for Δn_{eff} of roughly +0.02 would be appropriate in the design, since a too high positive value increases the diffraction loss.

In an actual VCSEL cavity under operation, the generated heat causes an elevated temperature distribution and an associated additional refractive index gradient because of the thermo-optical

Optics EXPRESS

effect. For the semiconductors we study, the thermo-optic coefficients are positive and thus lead to thermal lensing. Considering the sensitivity of lateral leakage to changes in refractive index caused by small changes in structure, it is natural to ask whether the small refractive index change caused by thermal lensing can further influence the lateral leakage. Therefore, in this study we have modelled the temperature distribution in the VCSEL cavity and used the results in the optical simulation. The electrical model is a modification of the fairly sophisticated APSYS model, which is implemented in the commercial software from Crosslight Software Inc, including several effects that are uniquely characteristic of nitride materials such as strong spontaneous and piezoelectric internal polarization fields [13, 14]. However, acknowledging the uncertainties in parameter values and their dependence on processing conditions that are not yet fully understood, our target is not to make a very accurate prediction of, say, the threshold gain for a certain device. Rather, we want to establish the qualitative change in behavior – in threshold gain, sources of optical loss and modal discrimination – when thermal effects are included, to see if some conclusions from the cold cavity study need to be revised, including the rules-of-thumb for the cavity design. Therefore we will use the same temperature simulation for all cavities, although they differ in their material composition in the aperture region, which constitutes a very small fraction of the entire simulated cavity. We will also consider only one case of heating, corresponding to an operating condition of 10 V applied voltage (~100 kA/cm^2 injection current density) in the model. This rather arbitrary choice represents a case with significant heating, the temperature increase over the ambient being ~70°C in the active region of the cavity. It is however not an unreasonably high temperature increase, since VCSELs are required to be able to operate up to temperatures ~70°C [15] and continuous-wave operation of GaN VCSELs has been demonstrated up to 95°C [16].

2. Numerical models

Two separate numerical models were used for the simulations, one optical and one current/temperature model. Prior to the optical simulation, the electric current distribution was determined using the APSYS software. This software primarily solves the electrostatic potential distribution in the cavity, taking into account numerous higher-order effects that are characteristic for GaN. The calculated potential variation is the driving force for the current through the cavity, which in turn acts as a distributed heat source through Joule heating. The resulting elevated temperature distribution in the cavity was obtained from the spatial heat source distribution using COMSOL Multiphysics software to solve the stationary heat equation; the results were then fed into the optical model.

The optical model was described in detail in [12, 17], but for the present work it was modified to also accept a temperature distribution in the cavity as input. The optical model is a true 3D model based on a scheme very similar to that of the rigorous vectorial 3D method described in [19, 20]. However, because of the strongly paraxial field in a VCSEL cavity, the field is assumed to have only a transverse component. In this scheme the cavity is divided into segments in the longitudinal direction, within which there is no longitudinal variation of the cold-cavity refractive index. Within each segment, the back and forward propagating fields are calculated with beam propagation methods and are then connected to the adjacent segments by Fresnel reflections at the segment interfaces, a procedure which is iterated until a self-consistent solution is found. By suppressing the so obtained field solution, the field with the next lowest threshold gain can be found, i.e., one can obtain the performance also for the first higher order transverse mode. In the updated version, the given temperature distribution is converted to a corresponding change in refractive index, based on the thermo-optic coefficients of the different materials. Each segment is supposed to have a constant temperature, and thus change in refractive index, in the longitudinal direction, whereas in the radial direction both temperature and refractive index fall off. The temperature-induced change in refractive index is thus simply added to the

Optics EXPRESS

two-dimensional cold-cavity index distribution in each segment, and the iterative procedures follow as before. When a self-consistent update of the segment fields has been obtained, so that the monitored variables – wavelength (around 420 nm), mode field volume, and threshold gain in the quantum wells (QWs) – have converged, the cavity field is analyzed to determine the contributions from the different loss sources. In this post-processing step the values for the lateral loss, absorption loss and outcoupling loss through the top and bottom mirrors are determined.

In addition, the cold-cavity structure was also analyzed with a considerably simpler and quicker effective index method [18], which was also used in [19, 20]. This method yields as one of its results the so called effective index difference, Δn_{eff}, between the central and peripheral part of the cavity. The purpose of this calculation was only to extract Δn_{eff} for each of the studied VCSEL cavities to get a simple measure for how strongly guided the field is in that cavity; the higher the value for Δn_{eff}, the more strongly guiding is the cavity.

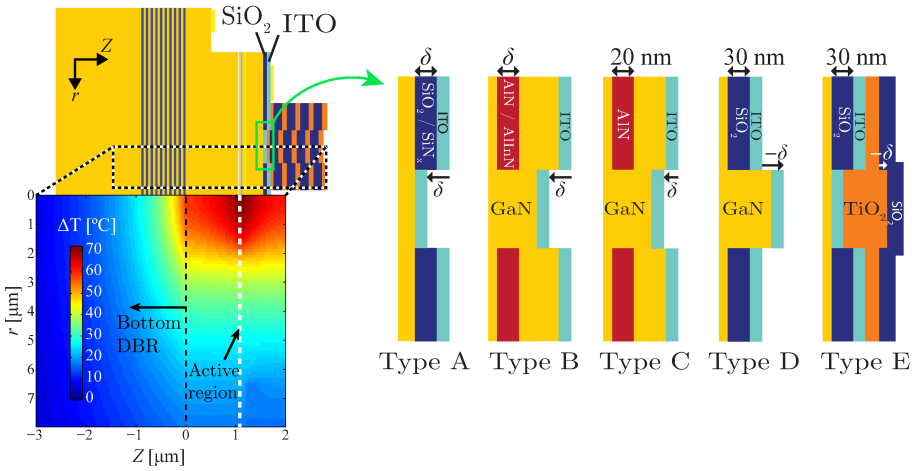

Fig. 2. Details of the layer structure in the different studied types of current apertures. For clarity, in the shown layer structures the ITO layer in the central region appears to be isolated from that in the periphery, but in reality the ITO-layer is continuous across the step-like structure created by the aperture [21]. Thus, the ITO always provides an electrical connection between the p-GaN and the metal p-contact. The definition of the step height δ in the topmost part of the layer structure is also indicated. The inset shows the calculated temperature distribution in the indicated part of the cavity.

3. Numerical simulations of the thermal lensing effects

The simulated cavity structures were the same as in [12], and represent different suggested, and partly experimentally tested, ways to realize the current aperture [1–4, 22–26]. Since it is mainly the step height that determines the behavior, as will be shown, similar results can be expected for BTJ VCSELs with an induced step height in the top DBR. Figure 1 shows the general features of the studied cavities, while Fig. 2 shows details of the structure in the vicinity of the current aperture. These details distinguish the different cavities, which were categorized into Types A-E. The step height is denoted by δ, and for the cavity types A-B the step height equals the thickness of the aperture layer, whereas for types C-E it is assumed that additional processing steps have been performed to reduce δ. The detailed layer structure and values for the most important material parameters are given in Table 1. The thermo-optic coefficients for

Optics EXPRESS

Table 1. Layer structure of the simulated VCSEL cavities, with material parameters used in the simulations.

Repeat	Material	Description	Thickness (nm)	Refractive index @420 nm, [Ref]	Absorption coefficient (cm^{-1})	Thermo-optic coefficient (K^{-1}), [Ref]
7×	TiO_2	Top DBR	40.1	2.62,*	0	-5×10^{-6}, [29]
	SiO_2	Top DBR	71.4	1.47,*	0	-5×10^{-6}, [29]
	TiO_2	Top DBR	25	2.62,*	0	-5×10^{-6}, [29]
	ITO	Current spreader	30	2.10,*	1000	1×10^{-4},†
	SiN_x /SiO_2 /AlN /AlInN	Peripheral part of current aperture	10–50	2.06,* 1.47,* 2.18,* 2.3, [27]	0	-5×10^{-6},† -5×10^{-6}, [29] 5×10^{-5}, [30] 1.5×10^{-4},†
	GaN	Contact layer	140	2.49, [28]	10	2.88×10^{-4}, [29]
	$Al_{0.2}Ga_{0.8}N$	Electron blocking layer (EBL)	20	2.42, [28]	0	5.7×10^{-5}, [29]
	GaN	Contact layer	13	2.49, [28]	0	2.88×10^{-4}, [29]
3×	$In_{0.03}Ga_{0.97}N$	QW barrier	6	2.68,†	0	2.58×10^{-4}, [29]
	$In_{0.1}Ga_{0.9}N$	QW	5	3,†	0	2.58×10^{-4}, [29]
	$In_{0.03}Ga_{0.97}N$	QW barrier	6	2.68,†	0	2.58×10^{-4}, [29]
	GaN	Contact layer	946.6	2.49, [28]	10	2.88×10^{-4}, [29]
42×	GaN	Bottom DBR	42.17	2.49, [28]	10	2.88×10^{-4}, [29]
	$Al_{0.8}In_{0.2}N$	Bottom DBR	45.65	2.3, [27]	10	1.5×10^{-4},†
	GaN	Substrate		2.49, [28]	0	2.88×10^{-4}, [29]

* measured values; † assumed values.

the dielectric materials are uncertain, with both positive and negative values appearing in the literature. However, they have no influence on the simulations since they are roughly two orders of magnitude smaller than that of GaN. The diameter of the current aperture was set to be 4 μm. The gain in the QWs was assumed to be spatially constant (at a value determined by the simulation) within this diameter and zero outside.

The material threshold gain in the QWs, required to sustain the cavity energy at a constant level, is shown in Fig. 3 for the fundamental mode. The threshold gain in cold cavity and cavity with thermal lensing are reported for all the considered cavity designs. As can be seen, thermal lensing leads to a significant reduction of the threshold gain for antiguided cavities, i.e., where $\Delta n_{\text{eff}} < 0$. This is in contrast to what could be intuitively expected: that thermal lensing would add (positive) guiding so that a strongly negatively guided cavity becomes less (net) guided; in other words that its Δn_{eff} is effectively increased towards zero where the cavity experiences higher loss which results in higher threshold gain. Clearly, this is not the case. Less surprising is that for cavities with moderate positive guiding, which have a minimum of both lateral leakage and diffraction loss already as cold cavities, thermal lensing has no appreciable effect. The insets in Fig. 3 show the total cavity field, and how the thermal lensing confines the central field to a

Optics EXPRESS

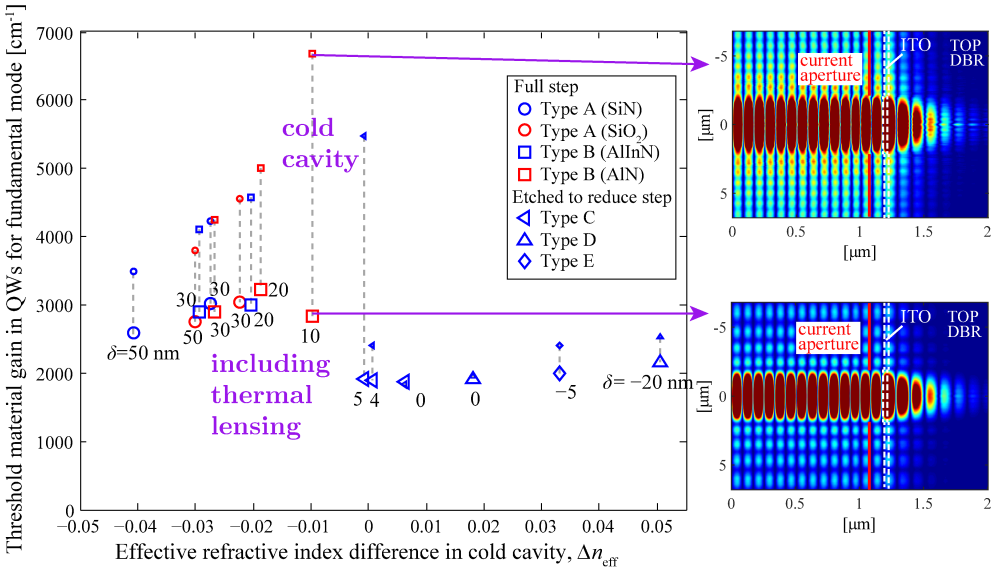

Fig. 3. Calculated material threshold gain in the three QWs for the fundamental mode in the studied cavities, with (large marker) and without (small marker) thermal effects. The number next to each larger marker denotes the layer step height (δ) for each case. The two insets on the right hand side show the amplitude of the cavity field for the indicated cavity, without and with thermal lensing included; only the part of the cavity that is above the bottom DBR is shown. To clearly show the peripheral fields, the central fields are shown saturated to the same degree in the two cases.

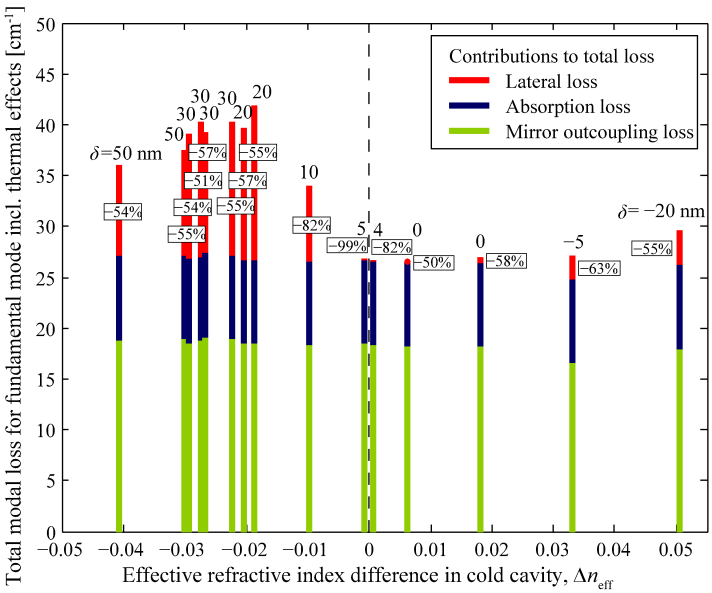

Fig. 4. Contributions to the total cavity loss for the fundamental mode in the studied cavities, with thermal effects included. The percentages denote the change in lateral loss compared to the cold-cavity case.

Optics EXPRESS

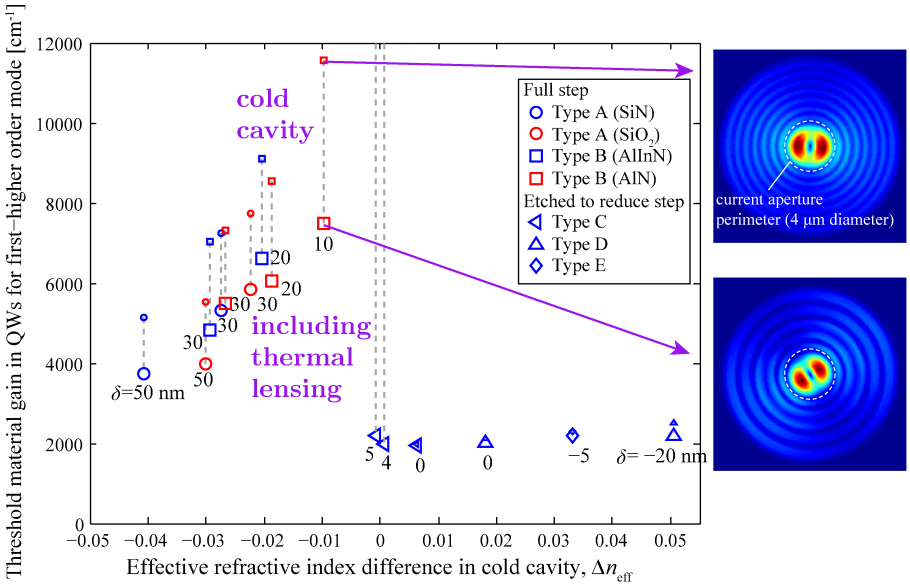

Fig. 5. The same as Fig. 3 but for the first-higher order mode. The insets show the cross-sectional intracavity field near the active region for the indicated cavities.

noticeably smaller diameter and reduces the peripheral field. The peripheral field consists of two counterpropagating and slightly diverging waves, which give rise to the dotted appearance of the total field in the radial direction. The denser dot pattern for the case without thermal lensing indicates a larger divergence angle, while thermal lensing has a rectifying effect on the peripheral field as will be described in Section 4.

The contributions to the cavity loss, with thermal effects included, are shown in Fig. 4. The percentages indicate the change of lateral loss relative to the cold-cavity case. The absorption loss and outcoupling loss (mirror loss) are virtually unaffected by thermal lensing so no numbers are given for these losses. The figure clearly shows the strong reduction of the lateral loss, typically by 50-60% and even more for the cavities closest to $\Delta n_{\text{eff}} = 0$, for which the lateral loss disappears almost completely. Clearly, it is the reduction of the lateral loss that causes the strong reduction in the threshold gain of the antiguided cavities, the causes of which will be analyzed in the next paragraph. These results should be compared to those for the first higher order mode, shown in Figs. 5 and 6; notice the difference in scales compared to the previous figures for the fundamental mode. First one can observe that thermal lensing makes lasing in the first higher order mode possible in all cavities, including the two closest to $\Delta n_{\text{eff}} = 0$ in which no higher-order mode exists in the cold cavity case. In the antiguided cavities, a similar significant reduction of the threshold gain occurs for the fundamental mode and for the first higher-order mode. However, the loss analysis reveals that the lateral loss reduction for antiguided cavities is slightly lower than for the fundamental mode, being typically 30-40%. This means the strong discrimination against higher-order modes that was observed for cold antiguided cavities remains also when thermal lensing is included. This is shown in Fig. 7 which shows the relative modal discrimination, i.e. the difference in threshold gain between the first-higher order and fundamental modes, divided by the threshold gain for the fundamental mode. For the antiguided cavities it is clear that the thermal effects lead to similar or even higher mode discrimination than for the cold cavity, with at least 40% higher threshold gain for the first higher order mode compared to the fundamental mode.

The simulations did not include carrier antiguiding, an effect which reduces the refractive

Optics EXPRESS

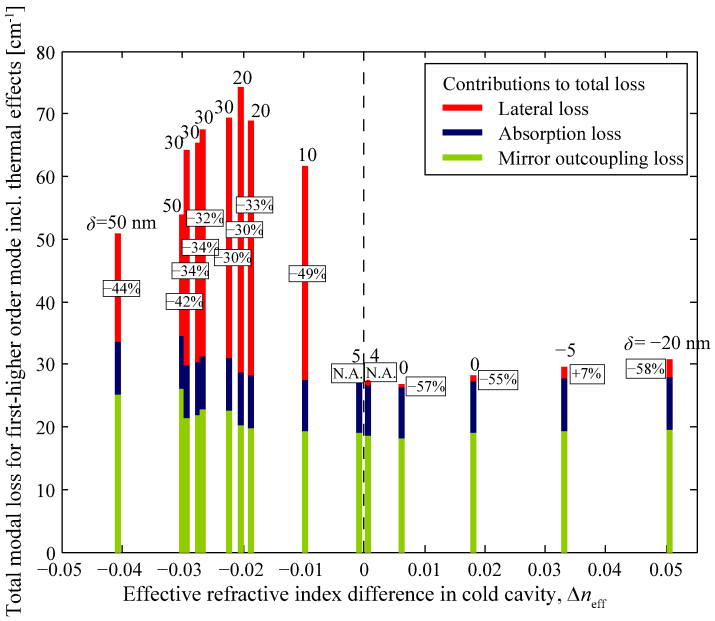

Fig. 6. The same as Fig. 4 but for the first-higher order mode.

index in the pumped part of the QWs due to the high concentration of carriers there. The value for the reduction of the refractive index as a function of the carrier density is not well known for gallium nitride materials [31, 32]. However, as a safety measure we recalculated the results for a few of the antiguided cavities using a quite large reduction of Δn=-0.5 of the material refractive index in the QWs within the diameter of the aperture, and none outside. In spite of this, there was no significant change in the results, indicating that under the studied conditions thermal lensing should be a far stronger effect than carrier antiguiding.

4. Explaining the effect of thermal lensing on lateral loss

For the cold cavity case a number of different viewpoints have been used to gain an intuitive understanding of the strong variation in lateral loss, and the associated variation in threshold gain, with the profile step. We previously found that the description by Hadley [18] was particularly simple, and allowed for a verification of the description based on the position of the side lobes in the far field [12]. Hadley's view is that the dramatic increase in lateral loss – the lateral leakage – that occurs when the cavity becomes antiguiding occurs because the peripheral cavity becomes resonant for an obliquely propagating wave at a certain angle to the optical axis. In the outcoupled field this preferential oblique propagation shows as the aforementioned distinct side lobe in the far field. The observation that the leakage shows a distinct decrease further into the antiguided region was explained from the fact that the propagation angle of the resonant wave increases. The field in the central part, which feeds the peripheral resonant field, has a lower angular field content at these more oblique angles and thus less light is being launched into the open resonant channel. Consequently, with this picture there are two possible explanations for the strong and robust reduction of the lateral leakage in the antiguided cavities when thermal effects are accounted for, as illustrated in Fig. 8:

(i) A less efficient launch of light from the central part of the cavity into the peripheral resonant wave. Presumably, this could happen if thermal lensing in the central part helps reduce the field components with an oblique propagation angle.

Optics EXPRESS

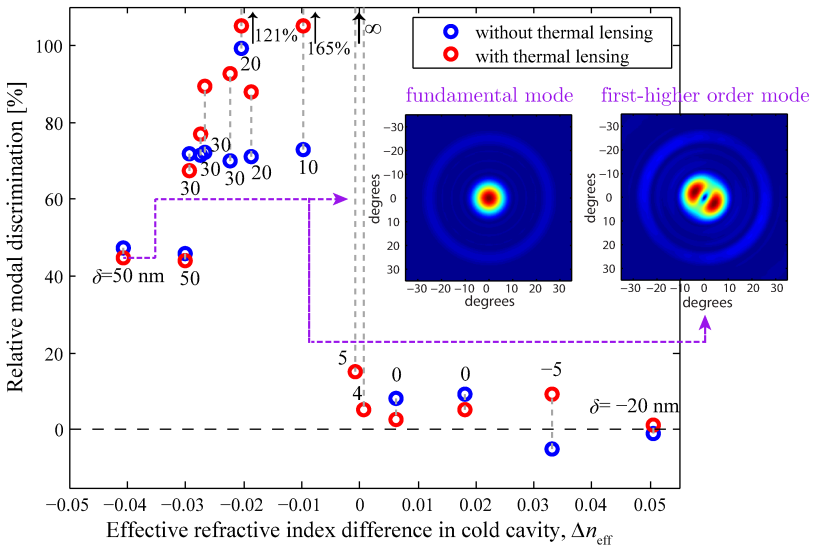

Fig. 7. The difference between threshold gain for the first-higher order mode and the fundamental mode, as a percentage of the threshold gain for the fundamental mode. To clearly show the details the two largest values for the relative modal discrimination, at 121% and 165%, are out of range on the vertical axis as indicated. The insets show the cross section of field distribution in the far-field, with the large-angle side lobe typical for strongly antiguided cavities, for the indicated cavity for both the fundamental and the first-higher order modes.

(ii) An inhibited propagation of the resonant wave in the peripheral cavity. Presumably, this could happen if thermal lensing in the peripheral part is strong enough and the propagation angle for the resonant peripheral wave is not too high. Then, as the wave propagates outwards in the peripheral region, the decreasing refractive index gradually rectifies the propagation so that it eventually becomes parallel with the optical axis and no further power escapes in the outwards radial direction; thus the field is being totally internally reflected and the peripheral structure works as a lossless circular waveguide.

To determine which explanation is correct the simulations for the fundamental mode were repeated again for all cavities. For each cavity two simulations were performed, each with a different, manipulated temperature distribution, see the insets in Fig. 8. One distribution had the correct temperature variation in the central part, whereas in the periphery there was no variation. The idea with this distribution, which gives thermal lensing in the central part but not in the periphery, is to test whether (i) is the primary effective mechanism in the reduced threshold gain when thermal effects are included. If so, the simulation with this temperature distribution and the actual one should give similar results. Likewise, the other manipulated temperature distribution, correct in the periphery but artificially held constant in the central part, should give thermal lensing in periphery but not in center. So if (ii) is the only effective mechanism, this distribution and the actual one should give similar results.

The results of the simulations are shown in Fig. 9, and compared with the previously shown cold cavity case and the case for the full thermal model with thermal lensing in both center and periphery. The results are striking in the clear distinction between the effects (i) and (ii): except for the region with very weak antiguiding, thermal lensing only in the periphery gives the same high threshold gain as for the cold cavity, whereas thermal lensing only in the center gives the same lower threshold as the full thermal lensing. In fact, with the single exception of the cavity with δ=10 nm, thermal lensing only in the central cavity gives the same low threshold as full

Optics EXPRESS

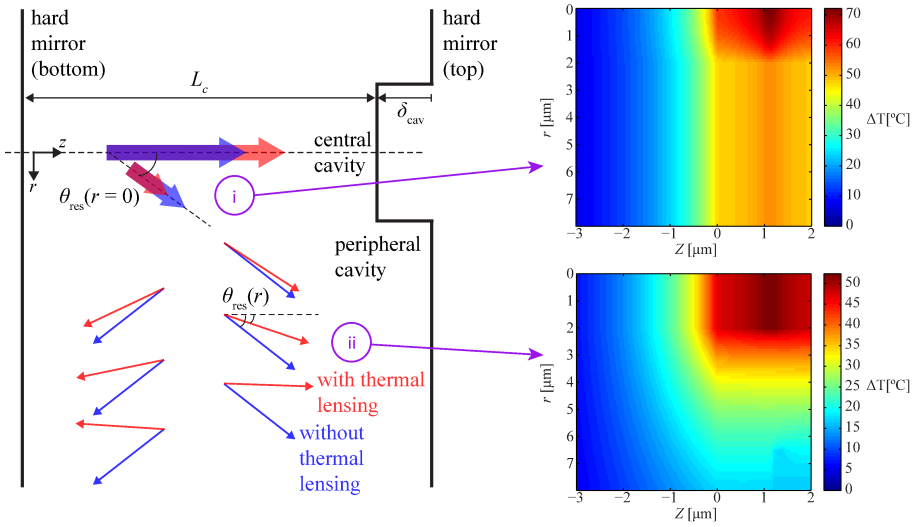

Fig. 8. The simplified hard-mirror model of the cavity, illustrating the two mechanisms (i) excitation from the central part of cavity, and (ii) resonant lateral transport in peripheral part of the cavity, that influence the lateral leakage. The insets show the manipulated temperature distributions used to separate the two mechanisms to determine which is "active" in a certain cavity.

thermal lensing in all cavities. Thus one can draw the conclusion that it is (i), the inhibition of light being launched from the central region, that is mainly responsible for the reduced lateral leakage – once the light is out in the peripheral part the thermal lensing in this part has no influence on the lateral loss. Only for weakly antiguiding cavities the situation may be different. For these cases the propagation angle of the resonant wave in the (cold) external cavity is small. This means that the radial decrease of the refractive index can straighten up the externally propagating field to the point where it becomes parallel with the optical axis and thus the lateral transport of energy stops, see Fig. 8. In other words, the peripheral cavity manages to confine the field laterally by total internal reflection because the launch angle of the resonant lightwave into the peripheral cavity is so small for weakly antiguided cavities. We can roughly estimate for which cavities this should happen by using the simple hard-mirror model depicted in Fig. 8. The model was previously used to verify the relation between launch angle and the strength of antiguiding, the latter given by the difference δ_{cav} in cavity length between the peripheral and central cavities, i.e. the height of the step in the profile of the top mirror [12]. Assuming that the central cavity is resonant for a field along the optical axis, the roundtrip condition for the phase is

$$2k_z L_c = 2k_0 n_c L_c = m_c \cdot 2\pi, \tag{1}$$

where k_z is the component of the wave vector in the z-direction, which is here the full k-vector since the propagation is along the optical axis, n_c is the refractive index in the central region and m_c is an integer. Likewise, in the peripheral cavity, the resonance condition for an obliquely travelling wave with propagation angle $\theta_{\mathrm{res}}(r)$ becomes

$$2k_z(L_c + \delta_{\mathrm{cav}}) = 2k_0 n_p(r)\cos(\theta_{\mathrm{res}}(r))(L_c + \delta_{\mathrm{cav}}) = m_p \cdot 2\pi, \tag{2}$$

where $n_p(r)$ is the local refractive index. Since δ_{cav} is small, it is natural to assume that the integer $m_p = m_c$. Because of thermal lensing, $n_p(r)$ decreases with the radial distance and therefore the angle that is needed for the resonance reduces. Assuming that for large enough

Optics EXPRESS

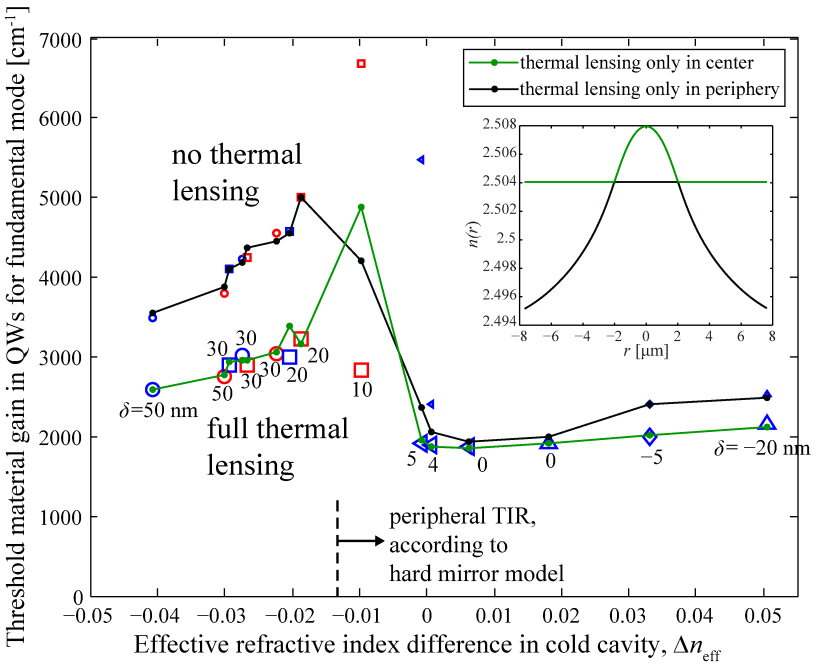

Fig. 9. Threshold gain for the fundamental mode for the manipulated temperature distributions. The values shown in Fig. 3 for the cold-cavity and for the actual temperature distribution are indicated for comparison. In this figure the onset of total internal reflection in the peripheral cavity according to the simplified hard-mirror model is also indicated. The inset shows the refractive index profile in the radial direction near the active region for the manipulated cases (same color code as in the main figure).

r the wave has become completely parallel with the optical axis, i.e., $\theta_{\mathrm{res}}(r)$=0, so that lateral transport completely ceases (total internal reflection). Equations. 1 and 2 give

$$\delta_{\mathrm{cav}} = \frac{L_c(n_c - n_p(r))}{n_p(r)}. \tag{3}$$

From the inset in Fig. 9, which shows the radial variation of the refractive index in a longitudinal position near the active region, it can be seen that the maximum value for the refractive index difference in parenthesis in Eq. 3 is roughly 0.01. Using the same value as in [12] for the effective cavity length L_c=2 μm, to account for field penetration into the bottom DBR, we thus obtain the maximum value of δ_{cav} for which total internal reflection occurs in the peripheral cavity, $\delta_{\mathrm{cav,max}}$=8 nm. To compare this with our simulation of real cavities one should note that the totally unguided case, δ_{cav}=0, corresponds to Δn_{eff} = 0 which occurs not for δ=0 but for δ approximately 4-5 nm, because the aperture contributes to some (positive) guiding. Therefore, adding this offset in δ to $\delta_{\mathrm{cav,max}}$ and allowing for some uncertainty stemming from our crude model, we might conclude that total internal reflection in the periphery should occur for values of δ smaller than 10-15 nm. This has been indicated in Fig. 9. Evidently, this estimation works remarkably well: the cavities with δ= 4, 5, and 10 nm are the only ones where thermal lensing in the periphery is effective in reducing the threshold gain compared to the cold cavity. The fact that for these cavities inclusion of thermal lensing also in the center reduces the threshold gain even more is mainly because this further narrows the intracavity field so that the lateral overlap with the gain region in the QWs is improved. For δ smaller than 4 nm the cavities are guided and therefore no lateral leakage occurs even in the absence of thermal effects, and so peripheral

Optics EXPRESS

thermal lensing is again ineffective in reducing lateral loss.

5. Conclusions

The present work answers the speculations that concluded our previous investigation of cold-cavity nitride-based VCSELs. First, thermal lensing does not simply "add positive guiding" in the sense that an antiguided cavity would shift closer to the unguided region of operation (i.e. the transition region between the antiguided and guided regions) when thermal effects are included. This would result in an increase in the threshold gain, which is not observed. Rather, thermal lensing always robustly lowers the threshold gain for all antiguided cavities. By using manipulated spatial temperature distributions, the reason for this was found to be the thermal lensing in the narrow central part of the cavity, which reduces the injection of optical power into the peripheral part of the cavity. Remarkably, in general the thermal lensing in the peripheral part – which even undergoes a higher temperature-induced change in refractive index than the central part – has no effect at all on lateral leakage loss and threshold gain. Thus it can be anticipated that these results are quite invariant to different heat sinking schemes, since the latter might influence the peripheral temperature distribution but only very slightly the central one.

Second, we previously noted that although the moderately positively guided ($\Delta n_{\mathrm{eff}} \simeq 0.2$) cavity would be preferred for its low threshold gain, the strongly antiguided regime was also of interest because it offered discrimination towards higher-order modes, something which the $\Delta n_{\mathrm{eff}} > 0$ cavities inherently do not. The present inclusion of thermal effects should strengthen this interest, because thermal lensing lowers the threshold gain for the fundamental mode in the strongly antiguided cavity. At the same time the same strong discrimination against the first-higher order mode as for the cold cavity is maintained.

In this context it can be noted that the nitride VCSELs that have been experimentally realized so far generally suffer from a low beam quality. This can be attributed to a tendency for the intracavity field to filament, i.e. to have a strongly and irregularly varying lateral distribution of the optical intensity, often concentrated in a few hot spots (a tendency which is further enhanced because these lasers so far needed a quite large aperture diameter to lase at all). Such intracavity field could be thought of as a higher-order mode stabilized by slight spatial fluctuations in the refractive index and gain. Therefore operating in the positively guided or in the strongly antiguided regime with its significant mode discrimination, may be a practical and efficient way to suppress filamentation and obtain a high-quality output beam.

Funding

Swedish Energy Agency (P39919-1); Swedish Foundation for Strategic Research (IB13-0004); Swedish Research Council; Department of Microtechnology and Nanoscience at Chalmers University of Technology.